Nat. Hazards Earth Syst. Sci. Discuss., 1, 2589–2632, 2013
www.nat-hazards-earth-syst-sci-discuss.net/1/2589/2013/
doi:10.5194/nhessd-1-2589-2013

Natural Hazards and Earth System Sciences
Discussions
Open Access

A reliability assessment of physical vulnerability of reinforced concrete walls loaded by snow avalanches

P. Favier[1,2], **D. Bertrand**[1], **N. Eckert**[2], **and M. Naaim**[2]

[1]INSA Lyon/LGCIE (Laboratoire de Génie Civil et Ingénierie Environnementale), Site Coulomb 2, Avenue A. Einstein 69621, Villeurbanne cedex, France
[2]IRSTEA, UR ETGR, Grenoble, France, 2 rue de la papeterie, BP76, 38402 Saint-Martind'Hères, France

Received: 16 April 2013 – Accepted: 1 May 2013 – Published: 7 June 2013

Correspondence to: P. Favier (philomene.favier@irstea.fr)

Published by Copernicus Publications on behalf of the European Geosciences Union.

Abstract

Snow avalanches are a threat to many kinds of elements (human beings, communication axes, structures, etc.) in mountain regions. For risk evaluation, the vulnerability assessment of civil engineering structures such as buildings and dwellings exposed to avalanches still needs to be improved. This paper presents an approach to determine the fragility curves associated with Reinforced Concrete (RC) structures loaded by typical avalanche pressures and provides quantitative results for different geometrical configurations. First, several mechanical limit states of the RC wall are defined using classical engineering approaches (Eurocodes – EC2), and the pressure of structure collapse is calculated from the usual yield line theory. Next, the failure probability is evaluated as a function of avalanche loading using a Monte Carlo approach, and sensitivity studies (Sobol indexes) are conducted to estimate the respective weight of the RC wall model inputs. Finally, fragility curves and relevant indicators such a their mean and fragility range are proposed for the different structure boundary conditions tested. The influence of the input distributions on the fragility curves is investigated. This shows the wider fragility range and/or the slight shift in the median that has to be considered when the possible correlation/non-Gaussian nature of the input distributions is accounted for.

1 Introduction

The increasing urban development in mountainous areas requires addressing hazard issues such as rockfalls, landslides and avalanches (Naaim et al., 2010). In addition to human casualties, the physical vulnerability of civil engineering structures is concerned by snow avalanche risk management. Depending on the external loading applied to the structure, that is to say the natural hazard considered (rockfall, landslide, earthquake, etc.), the physical vulnerability of civil engineering structures is usually assessed differently depending on the nature of the failure modes involved. If a relevant failure criterion

NHESSD

1, 2589–2632, 2013

is defined that represents the overall damage level of the structure, the potential failure of the system can be assessed and even its failure probability if the calculations are performed within a stochastic framework.

Avalanche risk mapping is often carried out combining probabilistic avalanche hazard quantification (e.g. Keylock, 2005; Eckert et al., 2010) and vulnerability (deterministic framework) or fragility (probabilistic framework) relations to assess individual risk for people (Arnalds et al., 2004) and buildings (Cappabianca et al., 2008). For instance, the Bayesian framework (Eckert et al., 2009, 2008; Pasanisi et al., 2012) makes it possible to take into account uncertainties in the statistical modeling assumptions and data availability. On the other hand, better defining vulnerability or fragility relations remains a challenge for the improvement of the integrated framework of avalanche risk assessment (Eckert et al., 2012).

A review of vulnerability approaches for alpine hazards (Papathoma-Köhle et al., 2010) mentioned various studies conducted to derive vulnerability relations. Several definitions have been proposed. One point of view is to define the vulnerability of a structure by its economic cost and not its physical damage (Fuchs et al., 2007), which can require to express a recovery cost (Mavrouli and Corominas, 2010). Another point of view suggests that human survival probability inside a building is commonly related to the vulnerability of the building itself by empirical relations (Jonasson et al., 1999; Barbolini et al., 2004). For instance, Wilhelm (1998) introduced thresholds to build vulnerability relations for five different construction types impacted by snow avalanches and Keylock and Barbolini (2001) proposed relating the vulnerability of buildings with their position in the avalanche path. More recently, Bertrand et al. (2010) suggested using a deterministic numerical simulation to assess the structural failure susceptibility of reinforced concrete (RC) structures.

To describe the failure probability of civil engineering structures exposed to snow avalanches and thus derive fragility curves, reliability approaches can be considered. For instance, in earthquake engineering (Ellingwood, 2001; Li and Ellingwood, 2007; Lagaros, 2008) or for RC structures subjected to blast loading (Low and Hao, 2001),

NHESSD
1, 2589–2632, 2013

the latter technique is often used. In hydraulic risk research, some studies focus on assessing dam safety using reliability methods (Peyras et al., 2012). Direct simulations (such as Monte Carlo methods) give robust results but can be time-consuming. As an alternative, simulation-based or surface approximation methods are used to avoid the direct calculation of the failure probability (Lemaire, 2005), but convergence of the algorithm can be cumbersome.

In the snow avalanche context, vulnerability relations are often derived from back-analyzed in situ data which are often very scarce. These relations give the fraction of destroyed buildings as a function of the avalanche loading. A reliability assessment of vulnerability relations (fragility curve derivation) is therefore a useful complementary tool for examining the interaction between the avalanche and the structures at different scales (avalanche path, urban area, individual house, etc.). This paper attempts to improve risk evaluations by proposing an innovative way to derive refined fragility curves that can be used in snow avalanche engineering.

As RC is the most usual material used to build structures exposed to potential avalanche loadings, herein we focus on this technology. First of all, the RC structure is described. Secondly, the mechanical model of the RC wall, the snow avalanche loading description and the damage level definitions are presented following by the statistical distributions of the inputs of the deterministic mechanical model. Finally, fragility curves are derived and their sensitivity to input parameters, modeling assumptions and failure criterion are discussed.

2 Methods

To protect people against snow avalanches, French hazard zoning defines three regions, which correspond to several levels of danger. The white zone corresponds to a safety zone where no potential interaction between the avalanche flow and the civil engineering structures can occur. In the red zone, the avalanche return period has been estimated at less than 100 yr and thus no construction is allowed. In the last

NHESSD
1, 2589–2632, 2013

zone (blue zone), civil engineering structures, such as buildings or houses, can be built only within certain restrictions. For the wall facing the avalanche, no opening is allowed and the wall has to resist at least a pressure of 30 kPa. Several technologies are available. As mentioned by Givry and Perfettini (2004) the most common are wooden, masonry, RC or mixed structures. RC technology appears to provide the best value for money. Moreover, RC is usually the most frequently encountered material for such structures and in particular for dwellings. The most vulnerable part of a structure built in an avalanche path is the wall facing the flow (Fig. 1). Thus, the damage of the entire structure can be assessed from the wall's resistance capacity. Indeed, the stress applied by the avalanche flow on the structure is balanced almost solely by the wall facing the avalanche. Hence, in order to overcome the complex problem of modeling the entire dwelling, only the structural elements carrying the load, i.e. a flat vertical RC wall, are considered in this work.

2.1 RC wall description

First, the features of the wall considered are presented (geometry, mechanical properties of reinforced concrete, boundary conditions). Then, the out-of-plane mechanical response of a RC wall is described. The nature of the damage and how it evolves over time as a function of the loading magnitude are presented. From the physical vulnerability assessment point of view, relevant performance functions dedicated to quantifying the damage level of the RC wall can be proposed. Finally, the wall loading due to a snow avalanche is presented and discussed.

2.1.1 RC wall features

The RC wall is composed of concrete and steel bars. The bars are orthogonal to one another and disposed homogeneously in the region of the wall where tensile stresses can develop (Fig. 1c). The number of steel bars is calculated from the steel density (ρ_s) needed to ensure the resistance of the RC wall. The usual sizes of dwelling houses

NHESSD
1, 2589–2632, 2013

situated in mountainous regions have been considered. Depending on the construction solution chosen, the RC wall boundary conditions can vary from one dwelling to another. Three kinds of boundary conditions are usually encountered. Each side of the wall can be considered either simply supported or clamped or can move without any constraint. From a mechanical point of view, concrete strength differs from compressive to tensile regimes. The characteristic compressive strength (f_{c28}) is generally ten times greater than the tensile strength (f_t). The compressive strength allowable for calculation is defined as f_{bc}, as a function of the loading time parameter θ and the security coefficient γ_b described below:

$$f_{bc} = \frac{0.85 \times f_{c28}}{\theta \gamma_b}. \quad (1)$$

Steel's behaviour exhibits two typical limits. First, the yield strength (f_y) corresponds to the development of permanent strain inside steel and secondly, the ultimate tensile strain (ε_{uk}) highlights the ability of steel to undergo more or less substantial yield strain before failure. The RC behaviour is a combination of the two materials. Figure 2 depicts the typical evolution of a RC member subjected to a monotonic loading. Four stages can be identified. The first stage represents the elastic response of the RC wall. The second stage corresponds to crack appearance and growth in the tensile zone of concrete. Once the crack distribution is stabilized (stage 3), the steel bars undergo plastic strain until the collapse of the RC element (stage 4). At the scale of the RC member, this last stage ends when a typical fracture lines pattern develops over the entire RC structure. This failure mechanism induces structure's loss of stability, leading to its collapse.

2.1.2 Limit states definitions

Appropriate quantitative performance functions are deduced from the RC wall damage levels. The structural failure is assumed to be due to excessive bending of the wall. The RC wall collapses under a bending failure mode. The first damage level is

NHESSD
1, 2589–2632, 2013

defined according to the crack appearance. The second and third damage levels are defined from Eurocode 2 design procedures (Mosley et al., 2007), where typical safety coefficients are proposed. Finally, the collapse of the RC wall is modeled by yield line theory (Johansen, 1962). It allows calculating the ultimate pressure that the structure can support before collapse. The first three stages are defined from the local mechanical balance of the cross-section where the highest bending moment arises, whereas stage 4 considers the whole failure pattern of the wall.

2.1.3 Elastic limit state

The first crack in the concrete defines the upper limit of stage 1. Beyond the first stage, the RC wall is no longer elastic. This limit is calculated from the bending moment leading to exceeding the tensile strength inside the concrete.

2.1.4 Ultimate Limit State (ULS)

This stage is defined in the Eurocode 2 regulation and concerns the safety of people in buildings and the building itself. In this paper, the ULS is related to potential loadings which can arise during the "normal" life term of the RC wall. The loadings are either permanent or transitory but not exceptional. Under bending, the ultimate limit state is obtained when either the concrete reaches its ultimate compressive strain or the steel its ultimate tensile strain. Usually, a RC member is designed to optimize its mass (thus its cost). Therefore, the cross-section is calculated to reach the ultimate strain limits inside concrete and steel at the same time.

2.1.5 Accidental Limit State (ALS)

The ALS differs from the ULS only in the loading description. Loadings are assumed exceptional (i.e. accidental). Thus, the probability of occurrence of such loadings is often low and explains why the safety factors are lower than in the ULS case (Table 1).

NHESSD
1, 2589–2632, 2013

2.1.6 Collapse

Finally, the collapse of the structure is characterized by its failure pattern. Under bending, failure lines develop through the RC member leading to the structure's collapse. In order to obtain the ultimate load, the yielding line theory is used, which is based on limit analysis theory; see for instance Nielsen and Hoang (2011). In the literature, some theoretical and experimental studies have been compared. They related collapse failure patterns as a function of boundary conditions (Sawczuk and Jaeger, 1963). Favre et al. (1990) provide theoretical solutions for RC slabs under various configurations.

2.1.7 Snow avalanche loading

Different types of avalanche flows can be observed in the Alps, inducing various loadings on the impacted structures. Spatial and temporal changes in snow avalanche loadings were experimentally observed and measured. For instance, small-scale experiments were conducted to reproduce the granular behaviour of snow and study its interaction with obstacles (Faug et al., 2010). Moreover, real-scale experiments were conducted, which allowed assessing the pressure magnitudes reached by dense avalanche flows (Thibert et al., 2008) and powder avalanches (Sovilla et al., 2008). An open question concerning the physical vulnerability assessment of civil engineering structures is whether the problem should be considered with a dynamical approach or a quasi-static approach. Various studies (Daudon et al., 2013) considered that the dynamic effect has to be taken into account, whereas others obtained vulnerability results assuming quasi-static approaches (Bertrand et al., 2010). As already suggested, the type of avalanche can control the type of flow loading (quasi-static or dynamic). To determine whether a dynamic or a quasi-static approach has to be considered, a modal analysis has to be performed to compare avalanche loading and structure characteristic times. In this paper, it is assumed that the pressure of the avalanche can be assumed to be quasi-static, as proposed by Bertrand et al. (2010). Moreover, a uniform pressure distribution is applied to the wall even if vertical variations

NHESSD
1, 2589–2632, 2013

are observed (Baroudi et al., 2011). The uniform pressure distribution could be considered as a safety factor, since the maximum is applied over the entire vertical whereas, in reality it decreases.

2.2 Mechanical approaches

Figure 3 depicts the transitions between each damage levels (Elas: elastic limit, ULS: ultimate limit state, ALS: accidental limit state, YLT: yield line theory). For each point, a loading pressure ($q_{\text{Elas}}, q_{\text{ULS}}, q_{\text{ALS}}, q_{\text{YLT}}$) can be calculated. For the first three cases, the load is obtained from the mechanical balance of the cross-section, which is submitted to the maximal bending moment inside the RC wall (Fig. 4). For the collapse load, yield line theory is used.

2.2.1 RC wall design under bending

2.2.2 Bending moment expression

First, the loss of RC elasticity is related to crack appearance when the tensile strength of concrete is exceeded. At this stage, the steel contribution in the overall behaviour can be ignored. The bending moment can thus be expressed as:

$$M_{\text{Elas}} = \frac{f_{\text{t}} \cdot I_x h^2}{6}. \quad (2)$$

The second (resp. third) damage limit is attained when the bending moment defined by the ULS (resp. ALS) is reached. In this case, the following assumptions are made:

- Sections remain plane during loading.
- No slip can occur between concrete and steel.
- The section evolves although the thickness in a linear fashion.

NHESSD
1, 2589–2632, 2013

– Concrete's tensile strength is ignored ($f_t = 0$).

– The ultimate compressive strain of the concrete (ϵ_{bc}) and the ultimate tensile strain of the steel (ϵ_{uk}) are respectively limited to 3.5 ‰ and 10 ‰.

As functions of the ULS and the ALS, concrete and steel change with the safety coefficients (γ_b and γ_s). As a consequence, the corresponding maximal bending moments also change. Figure 5 depicts assumed behaviours of the concrete and the steel. The RC wall design consists in attaining the maximum strengths in concrete and in the steel at the same time. f_{bc} (Eq. 1) is estimated: the loading time of an avalanche load is less than 1 h which implies $\theta = 0.85$ and the safety coefficient $\gamma_b = 1.15$. According to assumptions previously made, the Eurocode 2 supplies the coefficient $\mu_{AB} = 0.186$. Thus, by knowing the effective depth of the RC cross-section d, the corresponding moment per linear meter developed in the section can be calculated:

$$M_{AB} = \mu_{AB} d^2 f_{bc}. \tag{3}$$

Next, by knowing the lever arm $z \approx 0.9d$, the amount of steel (i.e. the percentage of steel inside concrete if normalized by the section area) needed to ensure that the balance of the bending moment is equal to:

$$A_s = \frac{M_{AB}}{z \frac{f_y}{\gamma_s}}, \tag{4}$$

where $\gamma_s = 1.15$ for ULS. Finally, the ULS and ALS ($\gamma_s = 1.0$) bending moments are expressed as:

$$M_{ULS} = M_{AB}, \tag{5}$$

$$M_{ALS} = A_s z \frac{f_y}{\gamma_s}. \tag{6}$$

NHESSD
1, 2589–2632, 2013

2.2.3 Boundary conditions

The spatial distribution of bending moments when the RC wall is submitted to a uniform pressure depends on the boundary conditions of each wall edge. Many combinations can be considered (free edge, clamped edge or simply supported edge). Bares (1969) proposed a useful abacus which gives the maximal bending moments developed in elastic rectangular plates for numerous configurations of boundary conditions. In this paper, the derivation of vulnerability relations is carried out within a reliability framework. Thus, to calculate the failure probability of the RC wall, many runs are needed. By using the abacus to assess the RC wall's resistance capacity, the computational time to perform a single run is very low, which makes it possible to use robust but computationally intensive reliability methods such as Monte Carlo simulations. Ten boundary conditions were implemented ((1)–(10), cf. Table 2). A linear spline is fitted to extrapolate coefficients from available coefficients provided by the abacus. Knowing the limit bending moment for each damage stage, the corresponding pressure is deduced for each direction x and y:

$$q^x = \frac{M}{\beta_x \times l_x^2}, \tag{7}$$

$$q^y = \frac{M}{\beta_y \times l_y^2}. \tag{8}$$

2.2.4 RC wall collapse (yield line theory)

The ultimate resistance capacity of RC slabs under uniformly distributed load can be derived from the classical yield-line theory (Johansen, 1962). This theory provides the collapse mechanism of the RC wall. Under an external loading, cracks will develop to form a pattern of "yield lines" until a mechanism is formed. A yield line corresponds to a nearly straight line along which a plastic hinge has developed because steel has reached its yield strength. To perform the yield line theory algorithm, the bending

NHESSD
1, 2589–2632, 2013

moment along yield lines needs to be characterized. The unitary bending moment along those lines remained constant and equal to the yielding steel moment calculated in Eq. (6). Indeed, as we are considering a uniform and isotropic reinforcement, the steadiness is verified. Then the energy balance between external and internal forces is assessed. According to the assumed yield line pattern, each neighbor plate can rotate. The plates rotate around axes defined by the edges of the slab and the yield lines. During the rotation, energy is dissipated inside the material by yielding. The dissipated energy is calculated as $M_{\mathrm{p}}^{i} \times \theta_i \times L_i$, where M_{p}^{i} is the plastic moment of the yield line considered i, θ_i the magnitude of the angle of rotation, and L_i the length of the yield line. The ultimate load is calculated from the equality between the external energy (W_{ext}) and the internal energy (W_{int}). In order to find the most likely collapse pattern, the kinematic theorem is used. It consists in determining the failure pattern minimizing the collapse load. Thus, the following equations are derived:

$$\begin{cases} W_{\mathrm{int}} = \sum_{i=1}^{n_{\mathrm{L}}} \overrightarrow{M_{\mathrm{p}}^{i}} \cdot \overrightarrow{\theta_i} \cdot L_i \\ W_{\mathrm{ext}} = q \iint \delta(x,y) \mathrm{d}x \mathrm{d}y \end{cases} \tag{9}$$

where n_{L} is the number of yield lines, $\delta(x,y)$ is the displacement matrix and q is the uniform load applied on the slab. Various failure patterns were considered as functions of the boundary conditions (Fig. 6). For each boundary condition, two failure patterns are mainly observed (Fig. 6, col. 2 and 3). Each pattern depends on an angle α_1 or α_2.

2.3 Reliability framework

The reliability concept is based on the fact that the structure's safety cannot be assessed deterministically because our knowledge of several properties of the studied system is imperfect.

NHESSD
1, 2589–2632, 2013

2.3.1 Failure probability definition

We wish to calculate the failure probability P_f defined as the probability for the resistance of the structure r to be less than or equal to a solicitation s:

$$P_f = P[r \leq s] = \int_{-\infty}^{s} f_R(r)\mathrm{d}r. \quad (10)$$

To solve Eq. (10), the probability density function of the resistance $f_R(r)$ needs to be known. The Monte Carlo methods is the randomized algorithm chosen. It is a time-consuming method, but a robust one. By randomly generating N variables from the input probability distributions, N mechanical runs can be calculated. Thus, the probability density function of the response can be approximated by the Monte Carlo integral: $\hat{P}_f$. The central limit theorem provides a $(1-\alpha)$ asymptotic confidence interval reflecting a significance level of α:

$$\hat{P}_f\left(1 - z_{1-\alpha/2}\frac{\sqrt{\hat{P}_f(1-\hat{P}_f)}}{\sqrt{N}}\right) \leq P_f \leq \hat{P}_f\left(1 + z_{1-\alpha/2}\frac{\sqrt{\hat{P}_f(1-\hat{P}_f)}}{\sqrt{N}}\right), \quad (11)$$

where $z_{1-\alpha/2}$ is the α-quantile of the normal distribution.

2.3.2 Sobol's index

Sobol's index is a tool providing the contribution of inputs to model outputs. It consists in quantifying the contribution of each input variable to the entire system's variability. It is based on a variance sensitivity analysis (Sobol, 2001). Saltelli et al. (2010) provide different numerical estimates and a comparison between their efficiency. For independent input variables, Sobol's first-order sensitivity coefficient S_i is equal to the

NHESSD
1, 2589–2632, 2013

total effect index S_{Ti}. Considering Y as the model output and $\boldsymbol{X}$ as the vector of inputs, Sobol's indexes are defined as:

$$S_i = \frac{V_{X_i}(E_{X_{\sim i}}(Y|X_i))}{V(Y)}, \tag{12}$$

$$S_{\mathrm{Ti}} = 1 - \frac{V_{X_{\sim i}}(E_{X_i}(Y|X_{\sim i}))}{V(Y)}. \tag{13}$$

According to Saltelli et al. (2010), Jansen (1999) provides the most efficient estimator of Eq. (13) through the approximation:

$$\hat{S}_{\mathrm{Ti}} = \frac{1}{2N}\sum_{j=1}^{N}\left(f(\mathbf{A})_j - f\left(\mathbf{A}_B^{(i)}\right)_j\right)^2, \tag{14}$$

where $Y = f(X_1, X_2, , X_k)$, $\mathbf{A}$ and $\mathbf{B}$ are an $N \times k$ matrix of input factors and $\mathbf{A}_B^{(i)}$ is a matrix where column i comes from matrix $\mathbf{B}$ and all other $k-1$ columns from matrix $\mathbf{A}$.

2.4 Vulnerability assessment

Statistical distributions of inputs need to be established. For calculation, six input variables were chosen and their distributions were determined: l_x, l_y, h(m), f_{c28}, f_{y}, and f_{t}. Two sets of distributions are used: a set of normal independent distributions and a more realistic and intricate one provided by the Joint Committee on Structural Safety (2001) (JCSS). Then, by building cumulative distribution functions of mechanical capacity load outputs, we can assess fragility curves.

NHESSD
1, 2589–2632, 2013

2.4.1 Statistical description of inputs

2.4.2 Normal distributions

First, to analyze the effect of each variable separately, a normal distribution describes each variable. Low and Hao (2001) provided several references identifying distributions for material inputs involved in our reinforced concrete slab problem. Mirza and MacGregor (1979) assumed normal distributions to model the variability/uncertainty regarding the dimensions of slabs. After in situ experiments, a 0.05 coefficient of variations is suggested and the designed value is adopted as the mean distribution value. To undergo a first statistical description for our model, a 0.05 coefficient of variation is assumed for all the inputs concerned, leading to the mean and standard deviation provided in (Table 3).

2.4.3 JCSS distributions

As reported by the JCSS, correlations between input variables can be taken into account. Steel's yield strength is still independent and follows a normal distribution. On the other hand, the tensile strength (f_t) and the compressive strength of the concrete (f_{bc}) distributions are deduced from the basic concrete compression strength (f_{c28}) distributions. For a ready-mixed concrete type with a $C25$ concrete grade, based on the given parameters, our parameters m, v, s, n are: $m = 3.65$, $v = 3.0$, $s = 0.12$, $n = 10$ and, t_v is a random variable from a Student distribution for v degrees of freedom:

$$f_{c28} = \exp\left(m + t_v s\left(1 + \frac{1}{n}\right)^{0.5}\right). \quad (15)$$

Then, f_t and f_{bc} are calculated with λ, Y_1 and, Y_2. λ is a factor taking into account the systematic variation of in situ compressive strength and the strength from standard tests. And $(Y_i)_{i=1,2}$ are log-normal variables representing additional variations due to

NHESSD
1, 2589–2632, 2013

special placing, curing, and hardening of the concrete. In our case, α_c is considered equal to $\frac{0.85}{\theta\gamma_b}$:

$$f_{bc} = \alpha_c f_{c28}^{\lambda} Y_1, \tag{16}$$

$$f_t = 0.3 f_{bc}^{2/3} Y_2. \tag{17}$$

For all parameters, the marginal mean and standard deviation were set according to the JCSS recommendation (Table 4). Difference with the previous case (Table 3) concerns (f_{c28}) for which they are higher in this case.

2.4.4 Normal correlated distributions

To implement an intermediate case, normal distributions are considered with a variance-covariance matrix deduced from the JCSS distributions. Means and variances of the six parameters l_x, l_y, h, f_{c28}, f_y, and f_t follow Table 3. The main correlation is the relation between f_{c28} and f_t: $\rho(f_{c28}, f_t) = 0.31$; others are lower than 0.01, i.e. close to independence.

2.4.5 Fragility curves derivation

A fragility curve $F(x)$ is a monotonic curve providing a failure probability as a function of a pressure applied, hence the cumulative distribution function $F(x)$ of the failure probability for the load x. The usual way to compute fragility curves is to set a pressure and vary the inputs from their statistical distributions. Thus, for each pressure a failure probability is obtained to build the fragility curve. Our approach is somewhat original as failure probabilities are derived from an inverse resolution. First, the structure capacity of resistance is found, then by abacus inversion, a load distribution is assessed. Finally, the cumulative distribution function of the latter distribution makes it possible to link a failure probability to a pressure. For instance, Fig. 7 depicts an output histogram of the ULS case for a rectangular wall with one free edge and three clamped edges with

NHESSD
1, 2589–2632, 2013

normal independent inputs and the fragility curve associated through its cumulative distribution function.

3 Results

3.1 Fragility curves with uncorrelated normally distributed inputs

3.1.1 Overview of all configurations

Using 10 000 runs per curve, smoothed fragility curves are obtained. Figure 8 depicts fragility curves according to the ten explored boundary conditions. They are sorted by the four failure criteria. Two visual groups are formed. First, all the curves representing the elastic limit state are gathered at low pressure loads. By considering the minimum 2.5 % quantile and their maximum 97.5 % quantile, their fragility range is [2.8, 27.2] (kPa). They do not interfere with fragility curves of the other failure criteria. On the other hand, the ULS, ALS and YLT fragility curves are defined on a range from 22.7 kPa to 218.6 kPa. It is interesting to note that the ALS fragility curves are scaled from the ULS curves by the security coefficient 1.15. This is easily explained by the definition itself of the ALS failure criterion.

Another point of view can be taken by plotting the same data according to the description of their boundary conditions (Fig. 9). Sets of fragility curves can be deduced. The four weakest structures present free edges. Rectangular walls with one free edge are sorted from the weakest by their boundary conditions as below: (1) one free edge and three supported edges, (2) one supported edge, two clamped edges and one free, (3) one clamped edge, two supported edges and one free[1] and (4) one free edge and three clamped edges. Then the second set of curves gathers the rectangular wall with supported edges ((5) four supported edges, (6) one clamped edge and three supported ones, (7) two supported edges and two clamped ones, (8) two supported edges and

[1] Exception for the YLT limit state where 3 and 4 are exchanged.

NHESSD
1, 2589–2632, 2013

two clamped edges side by side, (9) one supported edge and three clamped ones). Finally, the less vulnerable rectangular wall has four clamped edges. Equation (18) provides the p quantile of each vulnerability curve:

$$F(x) = \Pr(X \leq x) = p. \quad (18)$$

The previous equation allows considering a more quantitative approach. Table 5 sums up the 50 % quantiles and similar conclusions as described above are set up. The fragility range is defined as an interval: the lower bound is the 2.5 % quantile and the upper bound is the 97.5 % quantile of the fragility curve, which could be considered as very useful quantitative thresholds for engineering applications.

3.1.2 An example of one case: one free edge and three clamped edges

To investigate Monte Carlo confidence interval quantification, a focus on a particular case was required. The selected case is the rectangular wall with one free edge and three clamped edges (Fig. 10). The four limit state fragility curves can be distinguished together with Monte Carlo confidence intervals. As mechanical runs are not time-consuming, the number of calls N can be high enough to make numerical uncertainty negligible. Thus 10 000 runs induce thin confidence intervals near the curve, giving confidence in all the numerical results provided.

3.2 Parametric study

This section is devoted to the analysis of total Sobol indexes. As each of the input variables are independent, their sum is equal to 1. Sensitivity pies of outputs according to the input distribution can be plotted (Fig. 11). Four input parameters influence the fragility assessment based on the elastic failure criterion: f_t, l_x, l_y and h. The variable h is the predominant variable affecting the elastic-based failure probability. The ULS and ALS have the same sensitivity pies. Three input parameters are involved in the variability of ULS- and ALS-based failure probabilities: l_x, l_y and f_{c28}. f_{c28} seems to

NHESSD
1, 2589–2632, 2013

be the variable influenced the most by these outputs. This indicates which variables should be considered with the greatest care while designing a structure in practice, depending on the chosen failure criterion.

3.3 Correlated versus independent inputs

Fragility curves are highly dependent on the input distributions used. Outcomes were obtained from the three distributions previously described (Fig. 12). As a general overview, correlated distributions induce greater spread in fragility curves. Their fragility ranges have a higher amplitude than the range derived from a normal independent approach. Two explanations can be proposed. First, correlated distributions make mechanical variables evolve at the same tendency. Thus the whole system attains higher amplitudes. The second explanation lies in the number of variables considered: the more variables are considered, the more uncertainties are taken into account. It may be generalized that the more uncertainties are introduced in the input variables, the larger the fragility range of the fragility curves is. To ascertain and detail this conclusion, Fig. 13 focuses on the ULS example for the same boundary conditions. It appears clearly that from the deterministic point of view (a simple 0 – 1 response if the fragility limit is attained or is not attained) to the JCSS-based approach, fragility curves have wider fragility ranges. Quantiles at 2.5 %, 50 % and 97.5 % support these results (Table 6). Moreover, deterministic and normal distributions (whether or not they are correlated) have the same 50 % quantile. This results from the linear resolution of the mechanical process: the 50 % quantile remains constant whatever the covariance matrix, whereas the fragility range changes according to the normal distributions, marginal variances and correlations. On the other hand, a non-normal distribution (JCSS) induces a change in the 50 % quantile and in the fragility curve shape because of the non-symmetry of the joint input distribution. Note, however, that the non-Gaussian correlated case, despite its wider spread, shows a higher (and thus “safer”) modal value, so that simpler approaches (independent and correlated normal inputs) can be used in practice, at least as first approximations.

NHESSD
1, 2589–2632, 2013

4 Conclusions

The proposed approach can be considered as a comprehensive framework providing fragility curves for RC walls exposed to a snow avalanche pressure load. It could be considered with benefits for other sorts of problems and in particular for other types of civil engineering structures (structures with different materials, structures built with another technology, etc.) or natural hazards.

In detail, the influence of the boundary conditions and of the stochastic input distributions were systematically investigated, so as to provide robust fragility curves for various building types. Their most useful application may be individual risk assessment, including sensitivity analyses, for which the main concern is to evaluate the survival probability as a function of space for a hypothetical individual within different building types.

Four limit states based on the RC wall's mechanical response were considered, three local (cross-section scale) and one global (wall scale). For instance, the distinction between the ULS, concerning the safety of people, and the real collapse, where the structure is no longer standing, could lead to considering different thresholds for risk boundary assessment, leading to refined risk maps taking into account the winter usage of each building.

It has also been shown that, from a statistical point of view, stochastic input distributions strongly influence the shape of the fragility curves. Hence, independent or correlated variables and as well as the number of variables considered constitute important factors in the variability of fragility curves. This sensitivity to the input parameter distributions highlights that it seems important to consider and describe precisely the uncertainty sources for each application.

Finally, the deterministic simulations were carried out through simplified and effective mechanical models in terms of CPU time. This allowed using the Monte Carlo method, which gave robust results for the failure probability assessment. It should be noted, however, that more sophisticated mechanical models for civil engineering structures

NHESSD
1, 2589–2632, 2013

exist, based on the finite element (FE) method, which can simulate the structure in greater detail and in particular describe how the damage field evolves when material nonlinearities develop inside the concrete and the steel reinforcement. However, these FE models are often more complex (i.e. for assessing convergence) and time-consuming. Hence, they may be less well-adapted to a generic individual risk base approach, but more useful for studies deriving refined fragility curves for specific structures included in precise engineering projects.

Acknowledgements. The authors thank the research program MOPERA (Modélisation probabiliste pour l'Etude du Risque d'Avalanche – avalanches.irstea.fr/mopera-projet/) and the MAP3 ALCOTRA INTERREG program for financially supporting this work. Authors are also grateful to Regis Monnard for providing some pieces of advice.

References

Arnalds, P., Jónasson, K., and Sigurdsson, S. : Avalanche hazard zoning in Iceland based on individual risk, Ann. Glaciol., 38, 285–290, doi:10.3189/172756404781814816, 2004. 2591

Barbolini, M., Cappabianca, F., and Sailer, R.: Empirical estimate of vulnerability relations avalanche risk assessment, Manag. Informat. Syst., 9, 533–542, doi:10.2495/RISK040481, 2004. 2591

Bares, R.: Tables pour le calcul des dalles et des Parois, Dunod, Paris, 1969 (in French). 2599, 2623

Baroudi, D., Sovilla, B., and Thibert, E.: Effects of flow regime and sensor geometry on snow avalanche impact-pressure measurements, J. Claciol., 57, 277–288, 2011. 2597

Bertrand, D., Naaim, M., and Brun, M.: Physical vulnerability of reinforced concrete buildings impacted by snow avalanches, Nat. Hazards Earth Syst. Sci., 10, 1531–1545, doi:10.5194/nhess-10-1531-2010, 2010. 2591, 2596

Cappabianca, F., Barbolini, M., and Natale, L.: Snow avalanche risk assessment and mapping: a new method based on a combination of statistical analysis, avalanche dynamics simulation and empirically-based vulnerability relations integrated in a GIS platform, Cold Reg. Sci. Technol., 54, 193–205, 2008. 2591

NHESSD

1, 2589–2632, 2013

CEN, Eurocode 2: Design of concrete structures – Part 1-1: – general rules and rules for buildings (EN 1992-1-1:2004), CEN Technical Committee, 2005. 2613
Daudon, D., Baroth, J., Ma, Y., Perrotin, P., and Mommessin, M.: Sensitivity of a reinforced concrete protective gallery under a snow avalanche load, Struc. Saf., 41, 47–56, 2013. 2596
Eckert, N., Parent, E., Faug, T., and Naaim, M.: Optimal design under uncertainty of a passive defense structure against snow avalanches: from a general Bayesian framework to a simple analytical model, Nat. Hazards Earth Syst. Sci., 8, 1067–1081, doi:10.5194/nhess-8-1067-2008, 2008. 2591
Eckert, N., Parent, E., Faug, T., and Naaim, M.: Bayesian optimal design of an avalanche dam using a multivariate numerical avalanche model, Stoch. Env. Res. Risk A., 23, 1123–1141, 2009. 2591
Eckert, N., Naaim, M., and Parent, E.: Long-term avalanche hazard assessment with a Bayesian depth-averaged propagation model, J. Glaciol., 56, 563–586, 2010. 2591
Eckert, N., Keylock, C., Bertrand, D., Parent, E., Faug, T., Favier, P., and Naaim, M.: Quantitative risk and optimal design approaches in the snow avalanche field: review and extensions, Cold Reg. Sci. Technol., 79–80, 1–19, 2012. 2591
Ellingwood, B. R.: Earthquake risk assessment of building structures, Reliab. Eng. Syst. Safe., 74, 251–262, 2001. 2591
Faug, T., Chanut, B., Beguin, R., Naaim, M., Thibert, E., and Baroudi., D.: A simple analytical model for pressure on obstacles induced by snow avalanches, Ann. Glaciol., 51, 1–8, 2010. 2596
Favre, R., Jaccoud, J., Burdet, O., and Charif, H.: Dimensionnement des Structure en Béton – Aptitude au Service et Éléments de Structures, Presses Polytech. et Univ. Romandes, Lausanne, 1990. 2596, 2621
Fuchs, S., Thoeni, M., McAlpin, M. C., Gruber, U., and Bruendl, M.: Avalanche hazard mitigation strategies assessed by cost effectiveness analyses and cost benefit analyses – evidence from Davos, Switzerland, Nat. Hazards, 41, 113–129, 2007. 2591
Givry, M. and Perfettini, P.: Construire en montagne: la prise en compte du risque d'avalanche, Tech. rep., Ministère de l'écologie et du développement durable, 2004 (in French). 2593
Jansen, M.: Analysis of variance designs for model output, Comput. Phys. Commun., 117, 35–43, 1999. 2602
Johansen, K.: Yield Line Theory, Cement and Concrete Association London, London, UK, 1962. 2595, 2599

NHESSD
1, 2589–2632, 2013

Joint Committee on Structural Safety: Probabilistic Model Code, Part I–III, available at: http://www.jcss.byg.dtu.dk/, last access: 24 May 2013, 2001. 2602
Jonasson, K., Sigurosson, S. T., and Arnalds, D.: Estimation of avalanche risk, Report No. R99001-URO, Reykjavik, Veourstofu Islands, Reykjavik, VI-R99001-UR01, 44 pp., 1999. 2591
Keylock, C.: An alternative form for the statistical distribution of extreme avalanche runout distances, Cold Reg. Sci. Technol., 42, 185–193, 2005. 2591
Keylock, C. and Barbolini, M.: Snow avalanche impact pressure – vulnerability relations for use in risk assessment, Can. Geotech. J., 38, 227–238, 2001. 2591
Lagaros, N. D.: Probabilistic fragility analysis: A tool for assessing design rules of RC buildings, Earthq. Eng. Eng. Vib., 7, 45–56, 2008. 2591
Lemaire, M.: Fiabilité des Structures-couplage Mécano-fiabiliste Statique, Hermes, Paris, 2005. 2592
Li, Y. and Ellingwood, B. R.: Reliability of woodframe residential construction subjected to earthquakes, Struc. Saf., 29, 294–307, 2007. 2591
Low, H. Y. and Hao, H.: Reliability analysis of reinforced concrete slabs under explosive loading, Struc. Saf., 23, 157–178, 2001. 2591, 2603
Mavrouli, O. and Corominas, J.: Rockfall vulnerability assessment for reinforced concrete buildings, Nat. Hazards Earth Syst. Sci., 10, 2055–2066, doi:10.5194/nhess-10-2055-2010, 2010. 2591
Mirza, S. A. and MacGregor, J. G.: Variations in dimensions of reinforced concrete members, J. Struct. Div.-ASCE, 105, 751–766, 1979. 2603
Mosley, B., Bungey, J., and Hulse, R.: Reinforced Concrete Design: to Eurocode 2, 6th Edn., Palgrave Macmillan, UK, 2007. 2595
Naaim, M., Faug, T., Naaim, F., and Eckert, N.: Return period calculation and passive structure design at the Taconnaz avalanche path, France, Ann. Glaciol., 51, 89–97, 2010. 2590
Nielsen, M. and Hoang, L.: Limit analysis and concrete plasticity, CRC Press, Boca Raton, FL, USA, 2011. 2596
Papathoma-Köhle, M., Kappes, M., Keiler, M., and Glade, T.: Physical vulnerability assessment for alpine hazards: state of the art and future needs, Nat. Hazards, 58, 1–36, 2010. 2591
Pasanisi, A., Keller, M., and Parent, E.: Estimation of a quantity of interest in uncertainty analysis: some help from Bayesian decision theory, Reliab. Eng. Syst. Safe., 100, 93–101, 2012. 2591

NHESSD
1, 2589–2632, 2013

Peyras, L., Carvajal, C., Felix, H., Bacconnet, C., Royet, P., Becue, J.-P., and Boissier, D.: Probability-based assessment of dam safety using combined risk analysis and reliability methods-application to hazards studies, European Journal of Environmental and Civil Engineering (EJECE), 16, 795–817, 2012. 2592

Saltelli, A., Annoni, P., Azzini, I., Campolongo, F., Ratto, M., and Tarantola, S.: Variance based sensitivity analysis of model output, Design and estimator for the total sensitivity index, Comput. Phys. Commun., 181, 259–270, 2010. 2601, 2602

Sawczuk, A. and Jaeger, T.: Grenztragfähigkeits-Theorie der Flatten, Springer-Verlag Berlin/Göttingen/Heidelberg, 1963 (in German). 2596

Sobol, I.: Global sensitivity indices for nonlinear mathematical models and their Monte Carlo estimates, Math. Comput. Simulat., 55, 271–280, 2001. 2601

Sovilla, B., Schaer, M., and Rammer, L.: Measurements and analysis of full-scale avalanche impact pressure at the Vallee de la Sionne test site, Cold Reg. Sci. Technol., 51, 122–137, 2008. 2596

Thibert, E., Baroudi, D., Limam, A., and Berthet-Rambaud, P.: Avalanche impact pressure on an instrumented structure, Cold Reg. Sci. Technol., 54, 206–215, 2008. 2596

2591

Wilhelm, C.: Quantitative Risk Analysis for Evaluation of Avalanche Protection Projects, Norwegian Geotechnical Institute, Oslo, Norway, (1953) Revue, 1998.

NHESSD

1, 2589–2632, 2013

Table 1. Safety coefficients on steel and concrete strength for ULS and ALS calculations CEN (2005).

	ULS safety coefficient	ALS safety coefficient
Steel	$\gamma_s = 1.15$	$\gamma_s = 1$
Concrete	$\gamma_b = 1.5$	$\gamma_b = 1.15$

NHESSD
1, 2589–2632, 2013

Table 2. Maximum bending moment coefficients (β_x, β_y) for a rectangular plate subjected to an uniform load. The Poisson's ratio $\nu = 0.15$ and $\frac{l_x}{l_y} = 0.5$.

Boundary Conditions	β_x	β_y
(1) 4 simply supported edges	0.0991	0.0079
(2) simply supported on the 2 large edges clamped on the 2 small edges	0.0835	0.0088
(3) simply supported on one large edge clamped on the 3 other edges	0.0550	0.0045
(4) one free large edge clamped on the 3 other edges	$-\nu \times \beta_y$	0.0268
(5) one free large edge simply supported on the 3 other edges	$-\nu \times \beta_y$	0.0575
(6) clamped on one small edge simply supported on the 3 other edges	0.0908	0.0084
(7) simply supported side by side clamped on the 2 other edges	0.0570	0.0040
(8) 4 clamped edges	0.0405	0.0024
(9) one free large edge/one clamped large edge simply supported on the 2 small edges	$-\nu \times \beta_y$	0.0288
(10) one free large edge/one simply supported large edge clamped on the 2 small edges	$-\nu \times \beta_y$	0.0361

NHESSD
1, 2589–2632, 2013

Table 3. Table presenting the distribution parameters of material inputs.

Variable	Mean	Standard deviation
l_x(m)	8.0	0.4
l_y(m)	4.0	0.2
h(m)	0.2	0.01
f_{c28}(MPa)	30	1.5
f_y(MPa)	500×10^6	25×10^6
f_t(MPa)	2	0.1

NHESSD
1, 2589–2632, 2013

Table 4. Table presenting the distribution of independent material inputs.

Variable	Mean	Standard deviation
l_x(m)	8.0	0.4
l_y(m)	4.0	0.2
h(m)	0.2	0.01
f_y(MPa)	560×10^6	30×10^6

NHESSD
1, 2589–2632, 2013

Table 5. 50 % quantile of the CDF fragility curves according to boundary conditions and failure criterion, and (2.5 %, 97.5 %) quantile defining a fragility range (kPa).

Boundary Conditions	Elas	ULS	ALS	YLT
(1) 4 simply supported edges	8.4	60.2	69.3	97.0
	(6.5, 10.9)	(52.3, 69.1)	(60.2, 79.5)	(85.5, 109.5)
(2) simply supported on the 2 large edges	10.0	71.6	82.4	121.0
clamped on the 2 small edges	(7.7, 13.0)	(59.4, 87.6)	(68.3, 100.7)	(104.8, 139.1)
(3) simply supported on one large edge	15.2	108.6	124.9	158.5
clamped on the 3 other edges	(11.6, 19.7)	(95.0, 124.2)	(109.3, 142.8)	(138.8, 180.2)
(4) one free large edge	7.8	56.0	64.4	80.5
clamped on the 3 other edges	(6.0, 10.3)	(49.9, 63.7)	(57.4, 73.2)	(66.6, 96.7)
(5) one free large edge	3.6	26.0	29.9	38.1
simply supported on the 3 other edges	(2.8, 4.7)	(22.7, 29.6)	(26.1, 34.1)	(30.9, 46.7)
(6) clamped on one small edge	9.2	65.8	75.7	109.5
simply supported on the 3 other edges	(7.1, 11.9)	(56.0, 77.6)	(64.4, 89.2)	(95.6, 124.7)
(7) simply supported side by side	14.6	104.7	120.4	145.5
clamped on the 2 other edges	(11.2, 19.2)	(93.1, 117.6)	(107.1, 135.3)	(128.3, 164.4)
(8) 4 clamped edges	20.7	147.9	170.0	194.0
	(15.6, 27.5)	(133.3, 163.4)	(153.3, 187.9)	(171.1, 219.2)
(9) one free large edge/one clamped large edge	7.2	51.9	59.7	55.9
simply supported on the 2 small edges	(5.3, 10.3)	(43.2, 58.9)	(53.2, 67.8)	(47.2, 65.8)
(10) one free large edge/one simply supported large edge	5.8	41.4	47.6	60.9
clamped on the 2 small edges	(4.4, 7.5)	(33.5, 50.8)	(38.5, 58.5)	(48.9, 74.1)

NHESSD
1, 2589–2632, 2013

Table 6. Quantiles of fragility curves illustrated in Fig. 13.

Approach	2.5%	50%	97.5%
Deterministic		55.5	
Normal independent	50.2	56.3	64
JCSS	45.3	62.5	86.2
Correlated normal	33.9	56.6	79.6

NHESSD
1, 2589–2632, 2013

Table 7. Nomenclature.

ρ_s	density of steel
l_x	length of the slab
l_y	height of the slab
h	thickness of the slab
f_{c28}	cylinder characteristic compressive strength of concrete (age, 28 days)
f_{bc}	compressive strength of concrete
f_t	tensile strength of concrete
f_y	steel yield strength
ϵ_{uk}	ultimate tensile strain of the steel
γ_b, γ_s	safety coefficients on concrete and steel strength
$q_{ULS}, q_{ALS}, q_{Elas}, q_{YLT}$	characteristic loading at the ultimate limit state, at the accidental limit state, at the first cracks of the concrete in the tensile zone and at the collapse
ϵ_{bc}	ultimate compressive strain of the concrete
θ	loading time parameter
M_{AB}	rational dimensioning moment
μ_{AB}	ULS rational dimensioning coefficient
d	effective depth of the RC cross-section
z	lever arm in the section
β_y, β_x	Bares coefficient
ν	Poisson coefficient
W_{int}	internal virtual work
W_{ext}	external virtual work
n_L	number of yield lines
M_p^i	unitary plastic moment along the ith line
L_i	length of the ith line
θ_i	rotation angle of the ith element
$\delta(x,y)$	displacement matrix
q	uniform load
α_1, α_2	angles of YLT patterns
P_f	failure probability
r	resistance of the structure
s	solicitation
α	significance level of confidence interval
$f_R(r)$	probability density function of the resistance
S_i	first-order Sobol sensitivity coefficient
S_{Ti}	total Sobol sensitivity coefficient
α_c	coefficient from the JCSS distribution

NHESSD
1, 2589–2632, 2013

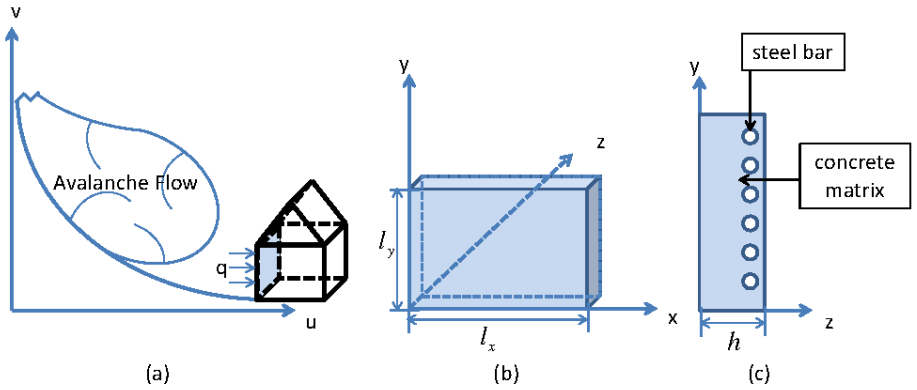

Fig. 1. Dwelling impacted by a snow avalanche **(a)**; RC wall geometry (**b** and **c**).

NHESSD
1, 2589–2632, 2013

A vulnerability assessment of RC walls loaded by avalanches

P. Favier et al.

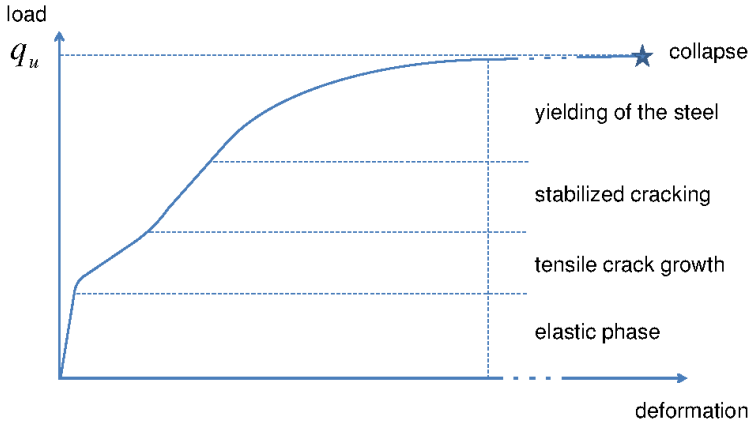

Fig. 2. Typical mechanical response of RC members submitted to a pushover test (monotonic loading until the collapse of the system), derived from (Favre et al., 1990, p. 343).

NHESSD
1, 2589–2632, 2013

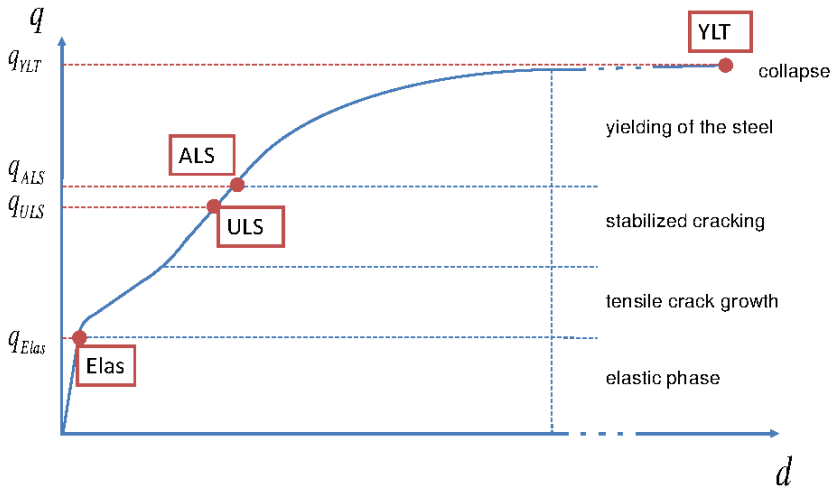

Fig. 3. Transitions between each damage levels (Elas: elastic limit, ULS: ultimate limit state, ALS: accidental limit state, YLT: yield line theory).

NHESSD
1, 2589–2632, 2013

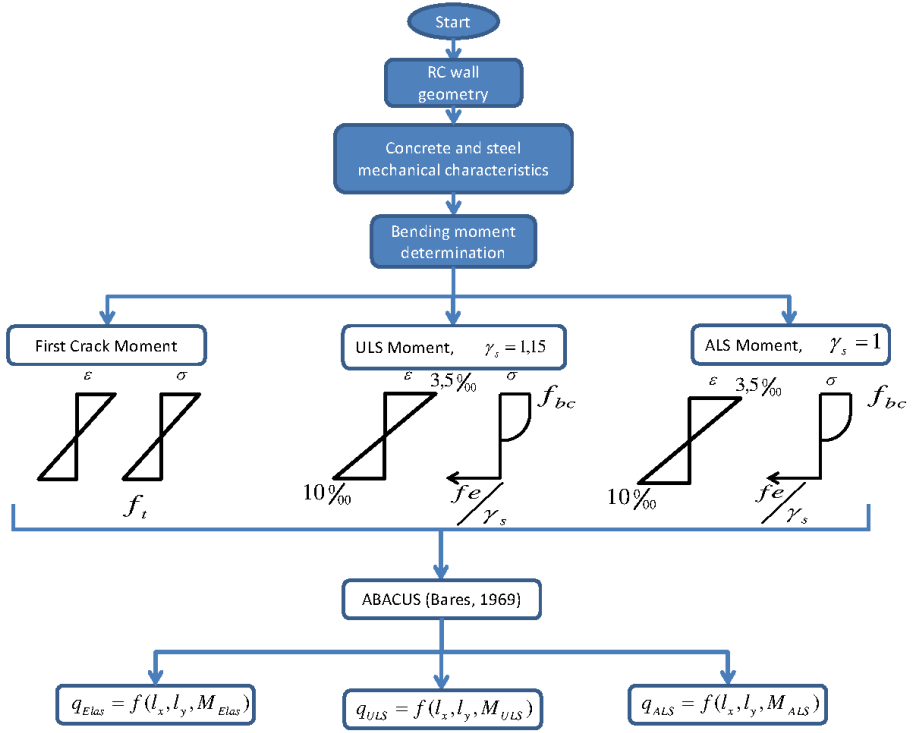

Fig. 4. Flowchart to calculate loading pressure related to each moment based on damage levels (Elas/ULS/ALS): first levels include geometry, mechanical characteristics and moment calculation; then, by inverting the Bares abacus (Bares, 1969), the corresponding loads are deduced.

NHESSD
1, 2589–2632, 2013

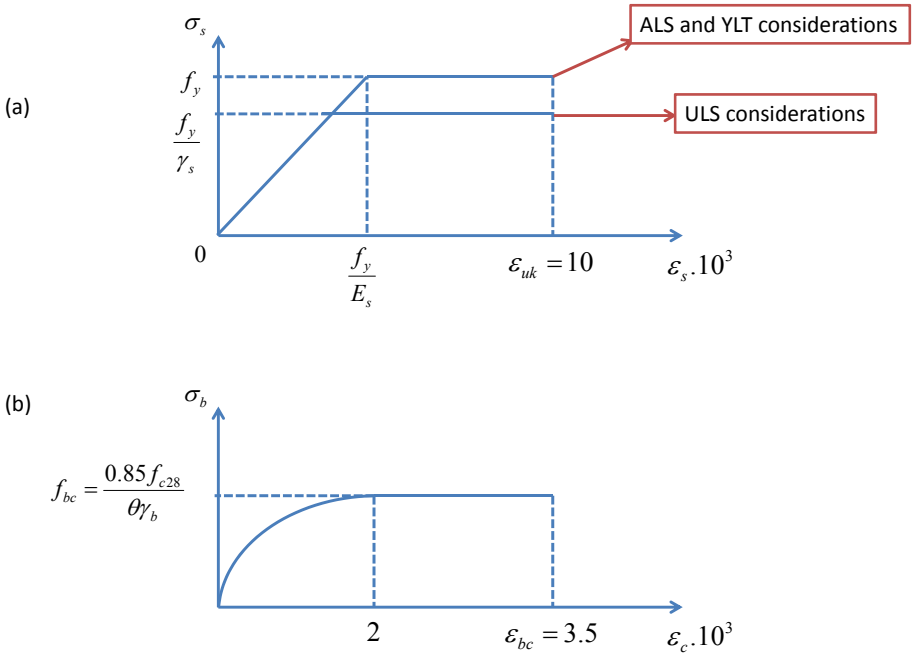

Fig. 5. Mechanical behaviour of the steel **(a)** and the concrete **(b)**.

NHESSD
1, 2589–2632, 2013

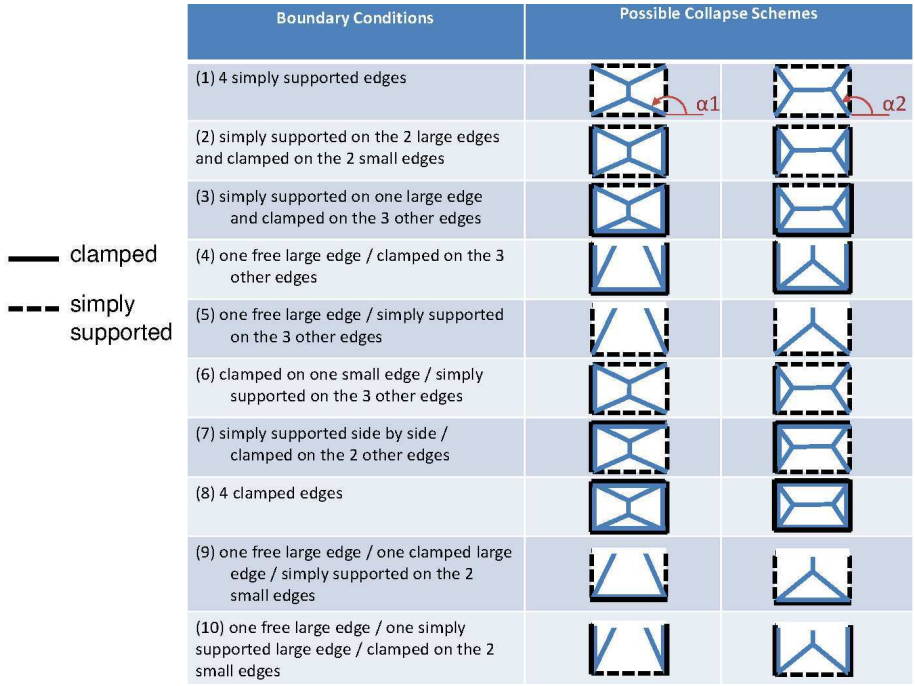

Fig. 6. Failure patterns according to several boundary conditions when considering yield line theory.

NHESSD
1, 2589–2632, 2013

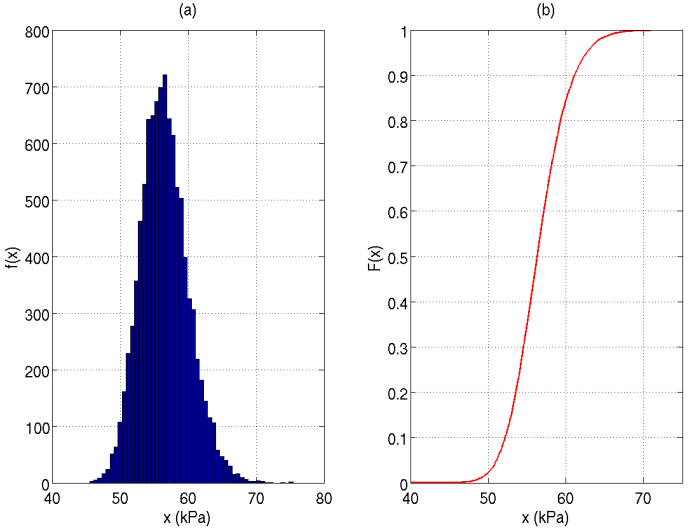

Fig. 7. Output histogram of the ULS case for a rectangular wall with one free edge and three clamped edges with normal independent inputs **(a)**, cumulative distribution function associated **(b)**.

NHESSD
1, 2589–2632, 2013

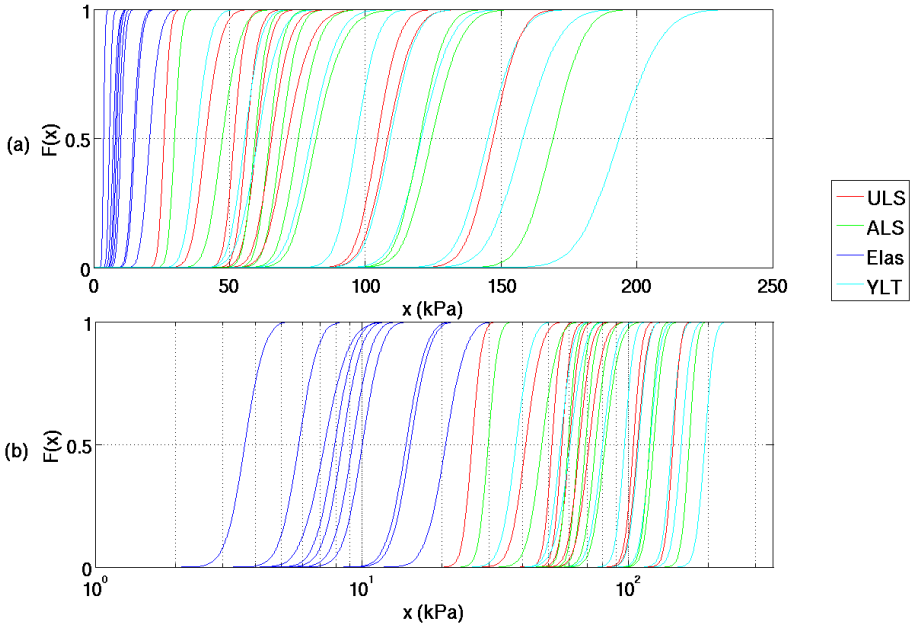

Fig. 8. Fragility curves according to boundary conditions sorted by failure criterion: **(a)** linear frame, **(b)** semi-log frame.

NHESSD
1, 2589–2632, 2013

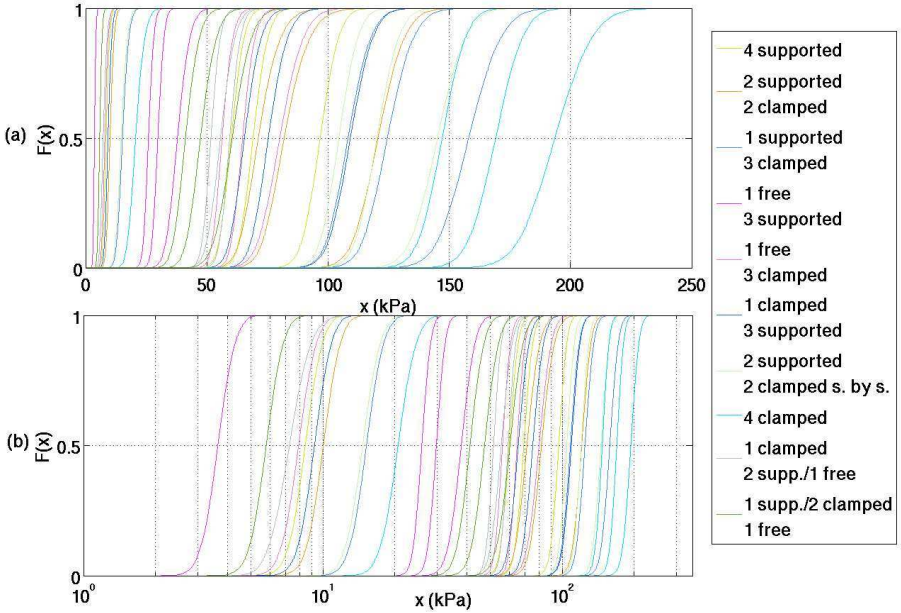

Fig. 9. Fragility curves according to boundary conditions sorted by boundary conditions: **(a)** linear frame, **(b)** semi-log frame.

NHESSD
1, 2589–2632, 2013

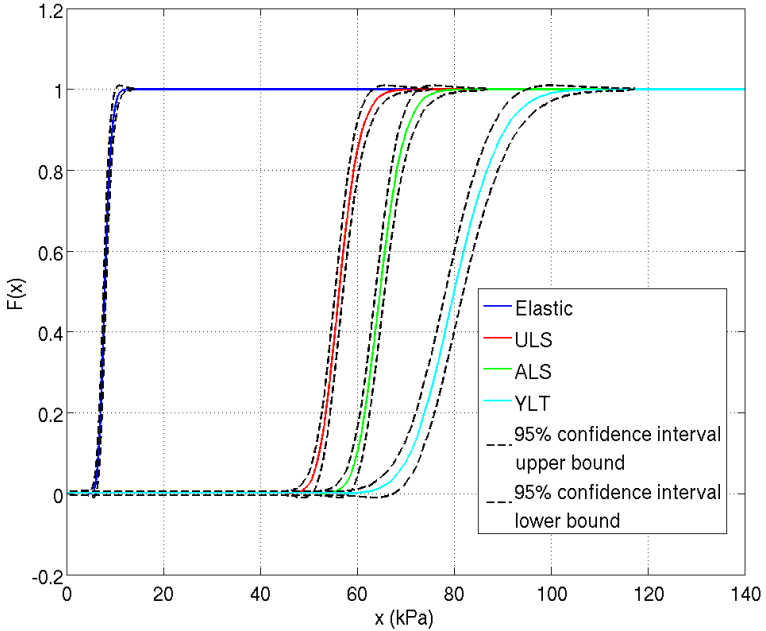

Fig. 10. Vulnerability curves and their 95 % confidence intervals from Monte Carlo simulations of a slab with one free edge and three clamped edges.

NHESSD
1, 2589–2632, 2013

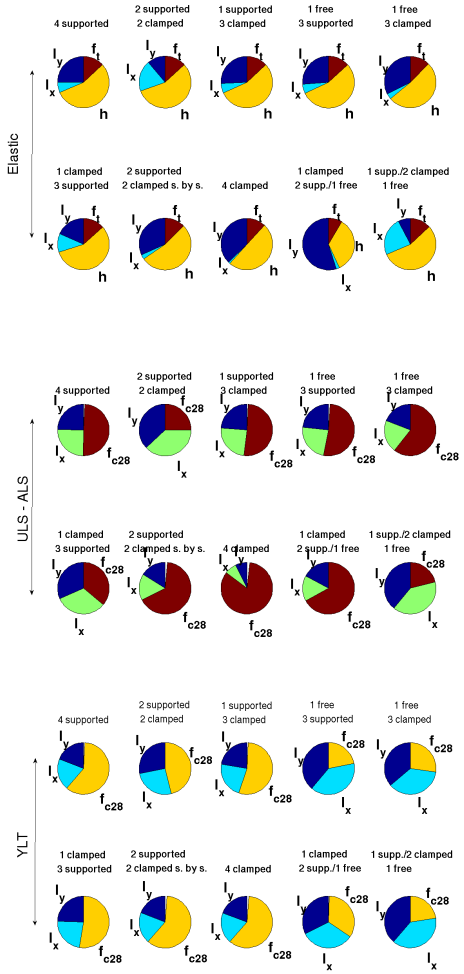

Fig. 11. Sensitivity pies for the Elastic, ULS (ALS) and YLT failure criteria.

NHESSD
1, 2589–2632, 2013

A vulnerability assessment of RC walls loaded by avalanches

P. Favier et al.

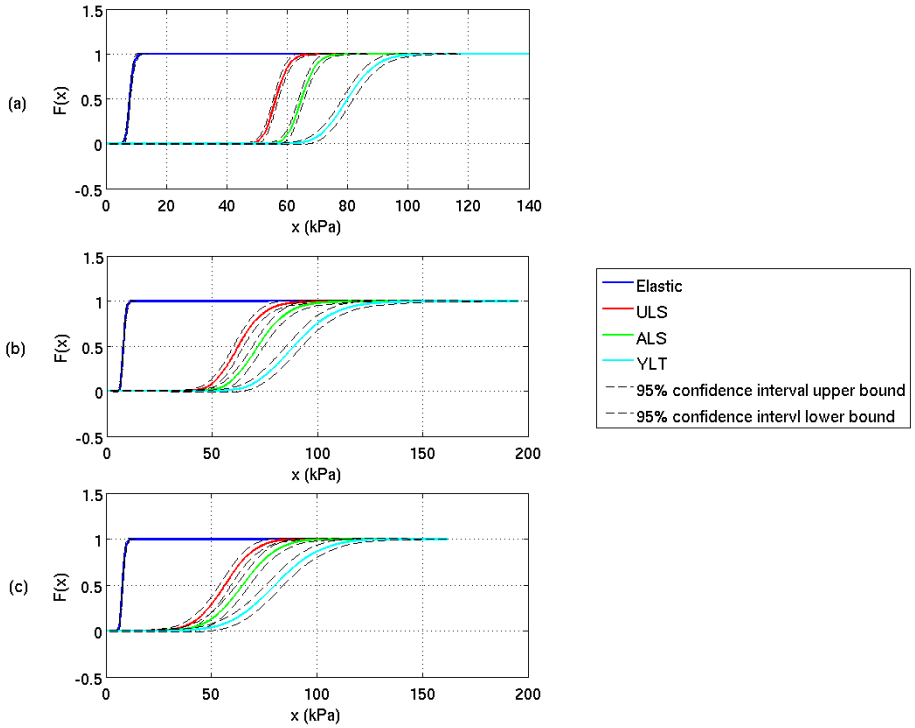

Fig. 12. Comparison of fragility curves from different input distributions of a slab with one free edge and three clamped edges: **(a)** normal independent distributions, **(b)** JCSS distribution, **(c)** correlated normal distribution.

NHESSD
1, 2589–2632, 2013

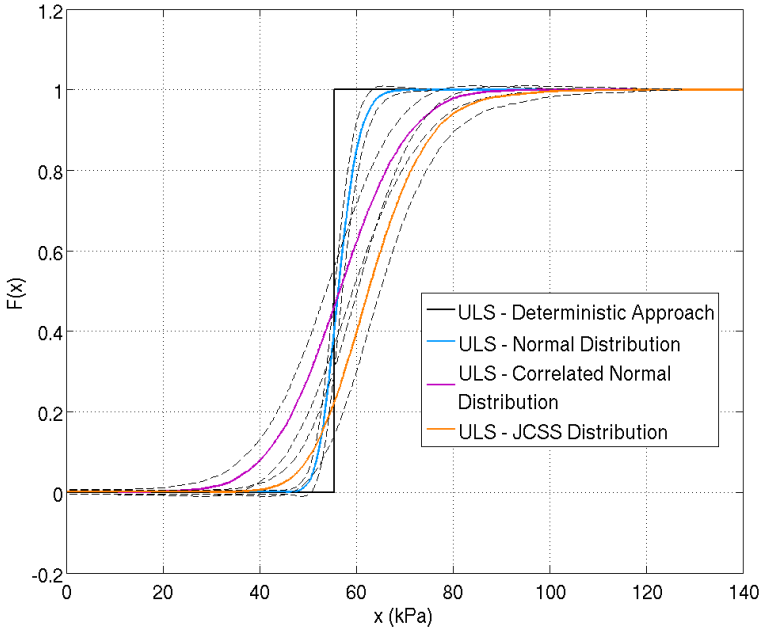

Fig. 13. Comparison between a deterministic approach and fragility curves from different input distributions and their 95% confidence intervals from Monte Carlo simulations, a slab with one free edge and three clamped edges under ULS considerations.

NHESSD
1, 2589–2632, 2013